Topological Features in Glyph-Based Corotation Visualization

Sohail Shafii, Harald Obermaier, Bernd Hamann, and Kenneth I. Joy

Abstract This chapter introduces a novel method for vortex detection in flow fields based on the corotation of line segments and glyph rendering. The corotation measure is defined as a point-symmetric scalar function on a sphere, suitable for direct representation in the form of a three-dimensional glyph. Appropriate placement of these glyphs in the domain of a flow field makes it possible to depict vortical features present in the flow. We demonstrate how topological analysis of this novel glyph-based representation of vortex features can reveal vortex characteristics that lie beyond the capabilities of visualization techniques that consider vortex direction and magnitude information only.

1 Introduction

The extraction and visualization of vortical features, such as vortex cores, has a long and successful history in fields such as aerodynamics. As new vortex definitions emerge, their visualizations are able to convey more characteristics associated with vortices. While the visualization of individual vortex cores by means of core line or hull extraction is successful in illustrating vortex direction and extent, it is limited in its capability to visualize more complex interactions between vortical features. We take advantage of a relatively new vortex descriptor, based on the concept of local corotation [1], to create a glyph-based visualization. This shape-based representation is an encoding of a spherical function that denotes strength of local corotation for arbitrary directions in space, and allows for the examination of vortices by means of a topological analysis. Automatic extraction and visual

S. Shafii (✉) • H. Obermaier • B. Hamann • K.I. Joy
Department of Computer Science, Institute for Data Analysis and Visualization,
University of California, Davis, CA 95616-8562, USA
e-mail: ssshafii@ucdavis.edu; hobermaier@ucdavis.edu; bhamann@ucdavis.edu;
kijoy@ucdavis.edu

P.-T. Bremer et al. (eds.), *Topological Methods in Data Analysis and Visualization III*,
Mathematics and Visualization, DOI 10.1007/978-3-319-04099-8_17,

analysis of maxima and corresponding topological regions in this representation provides insight into possible splitting or merging behavior.

This chapter is structured as follows. We first provide a summary of related work (Sect. 2) and analyze residual vorticity as a measure of local corotation (Sect. 3). Topological analysis of the created glyphs is presented in Sect. 4. We conclude by visualizing and analyzing two data sets.

2 Related Work

The work presented in this chapter spans the areas of glyph rendering and vortex visualization with a focus on analysis of topology. In the following we give a brief summary of related literature in these fields.

2.1 Vortex Extraction

Volumetric vortex features in flow fields may be extracted by a number of different vortex classifiers, such as the Q-criterion [2], the Δ-criterion [3–5] or the λ_2-criterion [6]. Kolář [7] introduced a residual vorticity method that not only removes the effects of shear by using the triple decomposition of the velocity-gradient tensor, but is also applicable to compressible flow fields. A similar paper by Kolář et al. [1] derived a simplification of this method using the *corotation of line segments*, which is the method that we discuss in this chapter. Since region-based methods do not readily create global vortical features, many have developed line-based techniques as an alternative. Examples are based on the parallel vectors operator [8], eigenvector analysis [9, 10], pressure-based predictor corrector schemes [11–13], ridge extraction [14, 15], or variations thereof [16–19]. Note that isosurface and medial-axis based representations allow for the visualization of complex vortex behaviors such as splitting. For a summary of various vortex detection methods, we refer to Post et al. [20] and Jiang et al. [21].

2.2 Vortex Visualization

The visualization of vortical features is mainly based on isosurfaces, line-like features from predictor-corrector, and skeleton or ridge extraction techniques [12]. Others [22, 23] use (flow) surface or voxel visualization techniques to verify and illustrate vortex cores. Topological analysis and visualization of vortex structures in combination with volume rendering was performed by Tricoche et al. [24].

2.3 Glyph Visualization

Glyphs, such as superquadrics [25], are frequently used to encode relevant quantities in vector [26, 27] and tensor fields [28]. Especially in medical visualization, topological properties of tensor glyphs are helpful to identify salient features in the data, such as fiber crossings in DW-MRI data [29,30]. These glyphs can be rendered as discrete meshes or, using modern graphics hardware, be ray-traced [31, 32]. A survey of gylph-based visualization techniques is discussed by Borgo et al. [33]. Our work introduces spherical glyphs as a novel approach to corotation-based vortex visualization. Topological features of these glyphs are evaluated and classified automatically to provide the means for a robust analysis of rotational properties and topological characteristics in vortical features. While previous vortex extraction approaches indicate the strength and directional components of vortices, they do not indicate all possible vortex directions that may exist at a point in a data set. Our glyphs provide a visual representation of vortex axes besides the dominant one that exists at a vortex, as that may indicate branching or merging behavior.

3 Corotation on a Sphere

The extraction of vortex cores relies on the availability of robust mathematical measures of flow rotation. In this work we investigate topological features of glyphs that are derived from a novel rotation measure known as *local corotation* or *residual vorticity*, as described in the following sections.

3.1 Physical Interpretation

Given a point $p \in \mathbb{R}^3$, the classic vorticity vector has two main properties. First, its direction corresponds to the normal of the plane along which two arbitrary line segments exhibit the maximal average angular velocity in the flow field [7]. Second, its magnitude represents twice the angular speed of the average rotation of these line segments. Residual vorticity [1], on the other hand, makes use of a similar physical interpretation with one significant difference: The residual vorticity vector is normal to the plane with maximal local corotation of line segments in a plane at p, for all possible planes at p. Instead of maximizing an average rotation speed, the residual vorticity technique maximizes a minimal common rotation speed. The difference of these two concepts is depicted in Fig. 1. Note that this alternative notion of rotation reduces the effect of strain and shear components on the computation of rotation directions.

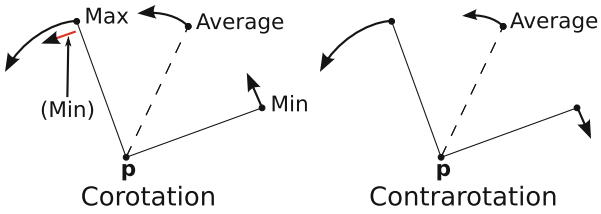

Fig. 1 An illustration of corotation and contrarotation of two line segments at a point p, based on Fig. 1 from Kolář et al. [1]. "Max" is the maximal rotation speed, while "average" and "min" are average and minimum rotational speeds in the corotation example, respectively. On the *left* we have corotation, where residual vorticity is the least absolute value angular velocity of the line segments shown (min). Average is just ordinary vorticity for both cases. Vorticity is still proportional to the average of all rotation speeds in the contrarotation example, which does not correspond to physical rotation in the plane

3.2 Local Corotation

The fact that residual vorticity is evaluated by maximizing local corotation over all possible plane orientations in 3D space makes it possible to analyze rotation in directions that do not correspond to the orientation with the globally maximal corotation. In the following we establish the mathematical background by describing how local corotation is defined for arbitrary orientations in 3D space.

Given a position $p \in \mathbb{R}^3$ in a velocity field $f : \mathbb{R}^3 \rightarrow \mathbb{R}^3$ with local gradient ∇f and an arbitrary orientation $v(\alpha, \beta) = (cos(\alpha) \cdot sin(\beta), sin(\alpha) \cdot sin(\beta), cos(\beta))$, quasiplanar residual vorticity as a measure of local corotation [1] is defined as:

$$\omega_{res}(\alpha, \beta) = sign(\omega(\alpha, \beta))(|\omega(\alpha, \beta)| - |s_D(\alpha, \beta)|), \tag{1}$$

where ω and S_D are the two-dimensional vorticity and deviatoric strain on the plane with normal v. Additionally, if $|\omega| \leqslant |s_D|$ then $\omega_{res} = 0$. Two-dimensional vorticity and deviatoric strain are computed as follows.

The quasiplanar effects of the velocity gradient tensor on an arbitrary plane with normal v is obtained by projecting the three-dimensional velocity gradient tensor into a two-dimensional coordinate frame orthogonal to v:

$$\nabla f^* = \begin{pmatrix} cos(\alpha) \cdot cos(\beta) & -sin(\alpha) \\ sin(\alpha) \cdot \cos(\beta) & cos(\alpha) \\ -sin(\beta) & 0 \end{pmatrix}^T \nabla f \begin{pmatrix} cos(\alpha) \cdot cos(\beta) & -sin(\alpha) \\ sin(\alpha) \cdot \cos(\beta) & cos(\alpha) \\ -sin(\beta) & 0 \end{pmatrix}. \tag{2}$$

With this two-dimensional velocity gradient tensor, quasiplanar vorticity and deviatoric strain are defined as:

$$\omega = \frac{\nabla f_{21}^* - \nabla f_{12}^*}{2} \quad \text{and} \quad S_D = \frac{\sqrt{(\nabla f_{11}^* - \nabla f_{22}^*)^2 + (\nabla f_{12}^* + \nabla f_{21}^*)^2}}{2} \tag{3}$$

As a result, local corotation in the form of residual vorticity can be defined for all positions v on a unit-sphere, with corotation scalar magnitude representing the minimal common angular rotation of line elements on a corresponding plane. In the following we visualize and analyze the spherical function given by ω_{res}.

4 Corotation Visualization and Topological Features

The fact that ω_{res} is capable of not only revealing the direction with maximal rotation, as commonly used for vortex core extraction, but the amount of rotation present in other directions in space makes it a prime candidate for detailed rotation analysis. We now discuss how we visualize the corotation function using spherical glyphs, and explain the various topological properties of these shapes.

4.1 Glyph Creation

Since positions on a unit sphere encode all possible orientations in 3D space, the complete domain of ω_{res} can be visualized by modifying such a spherical representation. Note that the spherical function ω_{res} may in theory be approximated as a higher-order tensor, allowing the application of existing glyph generation techniques, such as the one specified by Schultz and others [29, 30]. Such an approximation, however, is outside the scope of this chapter. The spherical meshes used in this work are created using icosahedron subdivision, as the resulting triangles of this mesh have equal areas and are suitable for easy level-of-detail control as shown by Schultz and Kindlmann [34]. Unlike a triangulation based on spherical coordinates, these triangles do not become distorted around the poles of the sphere.

A depiction of a spherical glyph is shown in Fig. 2, where corotation values are indicated by offsetting vertices of a unit sphere along the normal according to the local magnitude of ω_{res}. For this purpose, we first convert the Cartesian coordinates of each mesh vertex (relative to the center of the sphere) into a spherical coordinate representation, obtaining azimuthal and polar angles α and β, respectively. Next, we compute the mesh offset as the corotation scalar magnitude for the angle pair (α, β), and normalize the offset based on the range of corotation values over the entire sphere. We choose this type of local offset normalization over a global data-set-wide normalization, since exceptionally strong vortical features in flow simulations tend to lead to an unbalanced scaling. The offset value used per angle pair is the absolute value of ω_{res}, as we are interested in highest values of corotation magnitude that exist on the sphere.

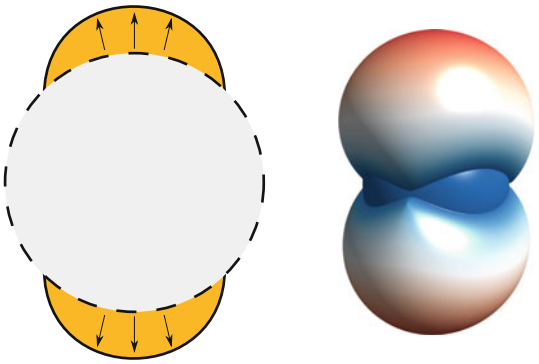

Fig. 2 Example of a spherical glyph, where its vertices are offset at positions where the corotation scalar magnitude is larger than zero. The *arrows* in the figure indicate where these non-zero values exist, while the base sphere (which corresponds to zero) is drawn with a *dashed line*. The colormap of the glyph varies from *blue* (weak corotation) to *red* (strong corotation)

4.2 Glyph and Function Properties

The scalar residual vorticity function and the resulting glyph representation have many interesting characteristics, some of which influence the applicability of topological methods as described in the next section. The ω_{res} function that defines the glyphs is specified in the domain $[0, \pi]$ for the angles α and β, and is periodic beyond that domain. As a result, the spherical glyph is point-symmetric with respect to its center, meaning that each extremum exists twice.

The variable behavior of the gradient magnitude of residual vorticity can often make the glyph-based representation difficult to predict. As a consequence, the shape of maximal regions in a glyph can vary strongly, and can include nearly flat regions with small gradient values, and peaks with extreme gradients. In addition, the use of absolute value and sign operators in the computation of residual vorticity introduces discontinuous derivatives. This can be observed in the form of C^0 continuous regions in glyph shapes. Large regions of the function may be zero, for directions where the field is not rotating, or deviatoric strain exceeds quasiplanar vorticity.

In general, i.e., when the flow field is not irrotational, ω_{res} has at least one maximum pointing along the direction of maximal rotation (two opposing maxima on the glyph representation). There are, however, multiple cases when additional local maxima can occur. The analysis of glyph topology with respect to the number of maxima present and shape characteristics of the corresponding topological regions can aid in understanding vortical features in the data set as described in the following section.

4.3 Topological Analysis of Individual Glyphs

The analysis of the topological properties of the glyph has the potential to indicate the existence of one or multiple related vortex directions. For instance, a glyph with two (opposing) peaks with two associated topological regions indicates that there is a vortex that runs through the center of the glyph, with the axis of the vortex being parallel to those peaks. Peaks that are associated with larger and less sharp topological regions indicate multiple rotation directions with a less distinct vortex core direction. If a glyph has additional maxima, then there exist additional vortex directions at those positions of the glyph, especially if the additional peaks are large relative to other peaks that exist. In the following we discuss methods for topological analysis of these glyphs and provide details about a sample implementation.

As mentioned in the previous section, the ω_{res} function and therefore the topology of the glyph shape may contain multiple local maxima. This property, coupled with the lack of C^1-continuity, precludes us from finding the maxima analytically. Furthermore, it is difficult to perform gradient ascent on this function because of the existence of sharp ridges (due to a discontinuous gradient), and because an ω_{res} function for a given ∇f tensor may have multiple maxima. In the latter case, it is challenging to find an appropriate seed point for gradient ascent that gives us the location of the global maximum. An alternative to finding a maximum explicitly could be based on ray-tracing, which is often used to represent the shape of a glyph. While it is possible to ray-trace the glyph in order to examine the topology of the glyph in image space, one will require a high-resolution image to make this analysis work and the analysis would be view-dependent. For these reasons, we employ an approximation of topological structures by directly examining the glyph meshes. One possible solution is to find local ω_{res} maxima within a neighborhood of the mesh. Unfortunately, it is difficult to perform such a maxima search with fixed neighborhood sizes due to the possible existence of high frequency features in the mesh.

We employ a watershed approach [35] instead, which effectively propagates the labels of maxima to other mesh vertices. We first sort all of the vertices of the mesh by function value, and identify the first vertex as a labeled maximum. As we move along the sorted list, we effectively move downwards in corotation value and identify vertices or "nodes" which are adjacent to labeled regions and which propagate those labels, or vertices where new maxima come into existence. We also track the merging behavior of regions with different labels by creating saddle points, which are assigned the label of the maximum with the largest ω_{res} value. We identify regions with nearly identical function values, or "plateaus," and treat these regions as single nodes during the labeling process. If there are multiple maxima connected via a large plateau, the plateau receives the label of the largest maximum and effectively connects it to the other maxima. After the watershed algorithm is completed, we create watershed graphs, which are similar to the "split trees" defined by Carr et al. [36]. We can filter the maxima of this tree that result from sampling artifacts, and color resulting descending manifolds of a glyph. An example of a glyph, and its corresponding unfiltered and filtered trees are shown in Fig. 3.

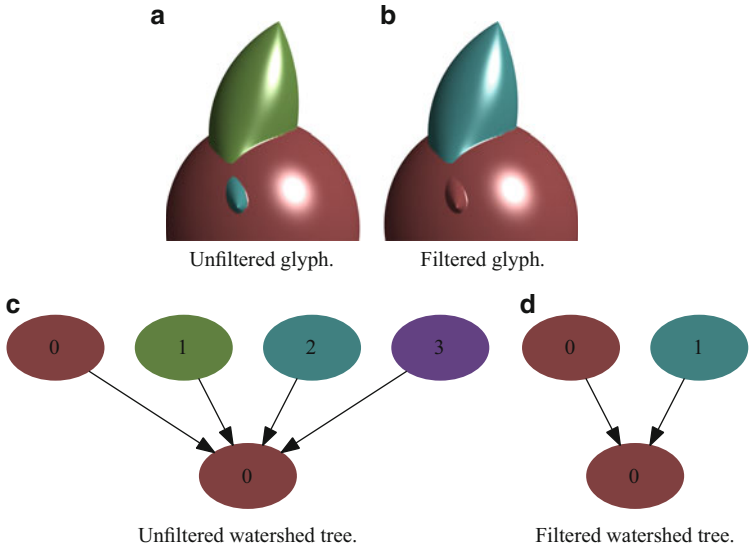

Fig. 3 Example of a glyph (**a**) along with its normal watershed tree (**c**), and the corresponding "filtered" representations (**b**), (**d**). The unfiltered versions contains small peaks, which include the diminutive, *teal-colored* maximum close to the center of the glyph in (**a**) and other (hidden from view) maxima. All maxima are connected to a large plateau (base icosahedron sphere). In the filtered versions, we removed small branches of the tree corresponding to these spurious maxima and subsequently recompute the topological regions

4.4 Topological Analysis of Multiple Glyphs

If multiple glyphs are positioned along a grid of a flow field, one can observe how their topological regions change as the field is traversed. In order to detect these changes, we first identify canonical glyph examples of various topologies that exist in the test data sets used in this chapter. In Fig. 4, we show these glyphs, and discuss how it is possible to have glyphs with well-defined or ambiguous directions for two or four peaks. Since the corotation function is symmetric, values beyond the domains $[0, \pi]$ for α and β are repeated in the graphs for this figure.

In Fig. 4a, c, e, g, we show visualizations and plots of large topological regions for two and four peaks, respectively. Each peak in these cases indicates multiple directions with strong rotations in large areas of the sphere. This is in stark contrast to Fig. 4b, d, f, h, where the pronounced peaks indicate unambiguous vortex directions for the two and four peak cases, respectively. It is notable how this glyph representation allows for the analysis of rotation in multiple directions, a feature that is not possible in classic direction and magnitude-based vortex visualizations.

Glyphs are likely to have two peaks that point along the forward and backward directions of the vortex core's axis at certain positions along a vortex core line, as seen in Fig. 4a, b. In other cases, glyphs might have four peaks (Fig. 4c, d), indicating

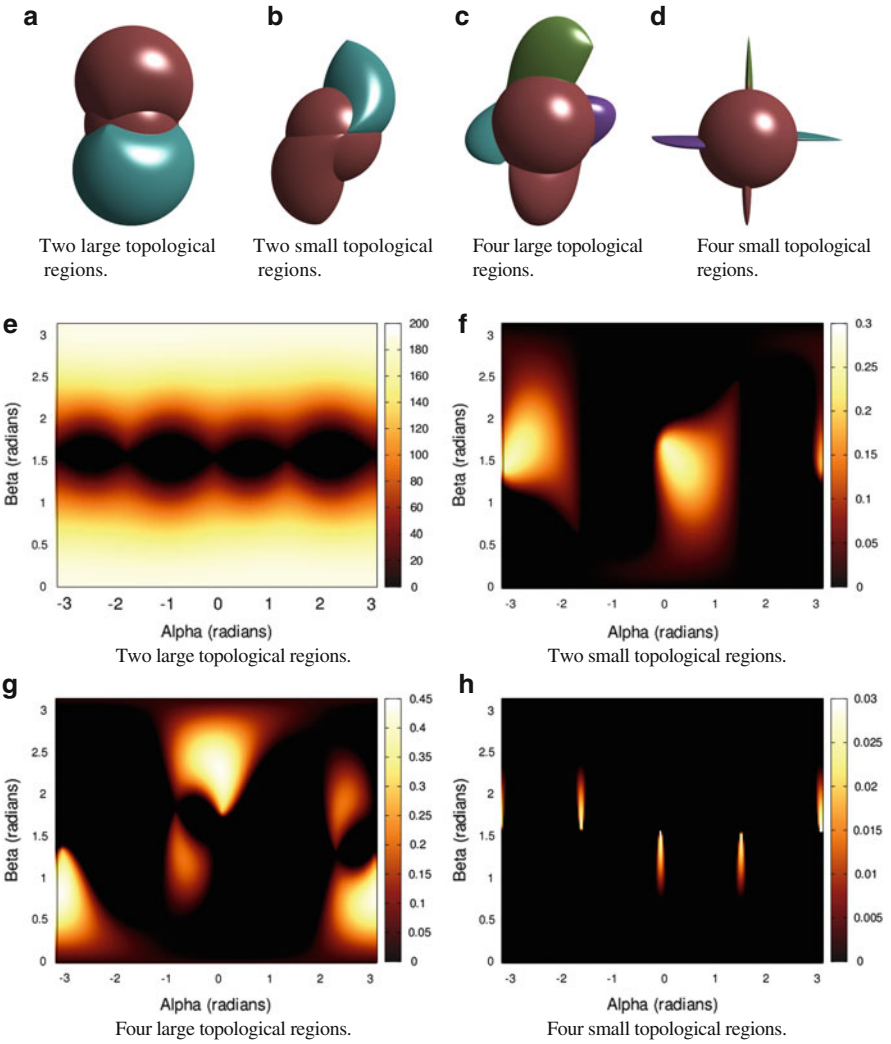

Fig. 4 Visualizations of various types of glyph topologies that we have observed, as well as their corresponding graphs (where the range of scalar corotation values is indicated by a color gradient of *black* to *yellow*). The corotation function is periodic, which explains why the visualizations and graphs portray symmetry. One can see that there may exist multiple directions with strong rotation close to the maximal corotation values in (**a**), (**e**), while in (**b**), (**f**) the maximum point is unique. Similarly, we observe four large topological regions in (**c**), (**g**), while we observe sharp, unambiguous peaks in (**d**), (**h**)

multiple orientations with maximal corotation. If the number of topological regions along a vortex increases from two to four, more vortex directions will start to appear. If two of the glyph's four peaks begin to wane, then the remaining two peaks will indicate dominating vortex directions. Additionally, the widening or narrowing of

individual topological regions indicate an increasing or decreasing number of vortex directions in the region of each peak, respectively.

5 Results

We have used our rendering technique to observe the topological behaviors of glyphs in our data sets. Our data sets include the "Blunt Fin" [37] and a von Kármán vortex street. The blunt fin data set is represented by a $40 \times 32 \times 32$ structured curvilinear grid, while the vortex street is represented by a $167 \times 34 \times 34$ structured curvilinear grid. The glyphs rendered are scaled based on the dimensions of the data set cell that they reside in. In these visualizations, topological regions are assigned individual colors. Sampled glyphs are excluded assuming their individual corotation ranges did not exceed a pre-specified threshold value.

5.1 Blunt Fin

We rendered our glyphs by uniformly sampling the data set as seen Fig. 5. In Fig. 5b, c, one can see that the many four-peak glyphs reside next to their two-peak counterparts. In Fig. 5d, e, we observe more instances of four-peak glyphs. The presence of this type of glyph indicates additional vortex directions that exist at this position. A standard vortex core line extraction technique only portrays the dominant vortex axis per point. In the future we hope to employ a sophisticated extraction technique to portray splitting or merging behaviors that could be related to these additional vortex directions.

5.2 Von Kármán Vortex Street

We visualized glyphs in the Von Kármán Vortex Street data set by uniformly sampling the grid as seen in Fig. 6. We observed glyphs near five stable vortex regions parallel to the y-axis of the data set, and the glyphs' peaks are aligned with the y-axis as we expected. Most of the glyphs' topologies are similar to their neighbors, and they mostly point in the same direction. This indicates a lack of additional vortex directions per glyph, a behavior that was present in the Blunt Fin data set.

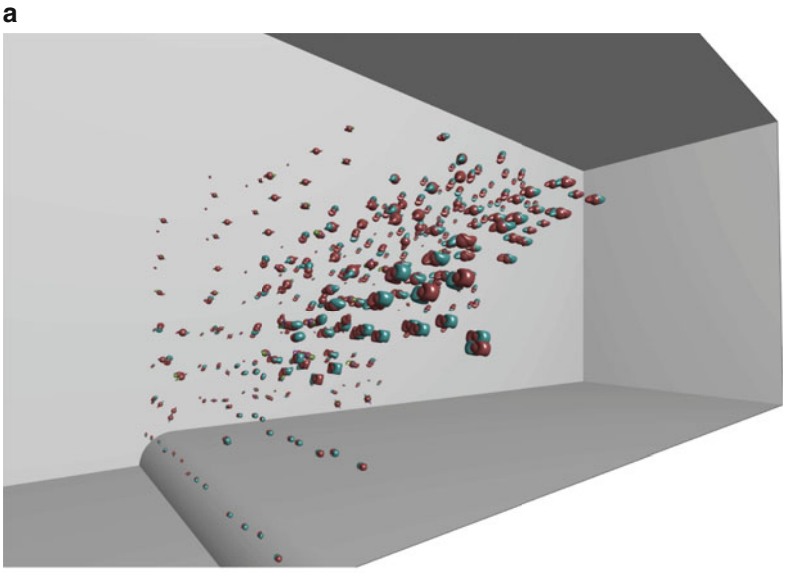

Overall visualization of Blunt Fin vortex cores and glyphs.

Close-up view of a Blunt Fin core with peaks identified.

Close-up view of a Blunt Fin core with corotation colormap.

Close-up view of a Blunt Fin core with peaks identified.

Close-up view of a Blunt Fin core with corotation colormap.

Fig. 5 Visualization of glyphs sampled uniformly in the Blunt Fin data set. The vortices in this data set are parallel with the blunt fin boundary and are parallel with the longest dimension of the data set. A visualization of most of the glyphs is shown in (**a**). The first close-up visualization is shown in (**b**), (**c**), where there exist many glyphs that possess four peaks. Figure (**d**), (**e**) show more four-peak glyphs

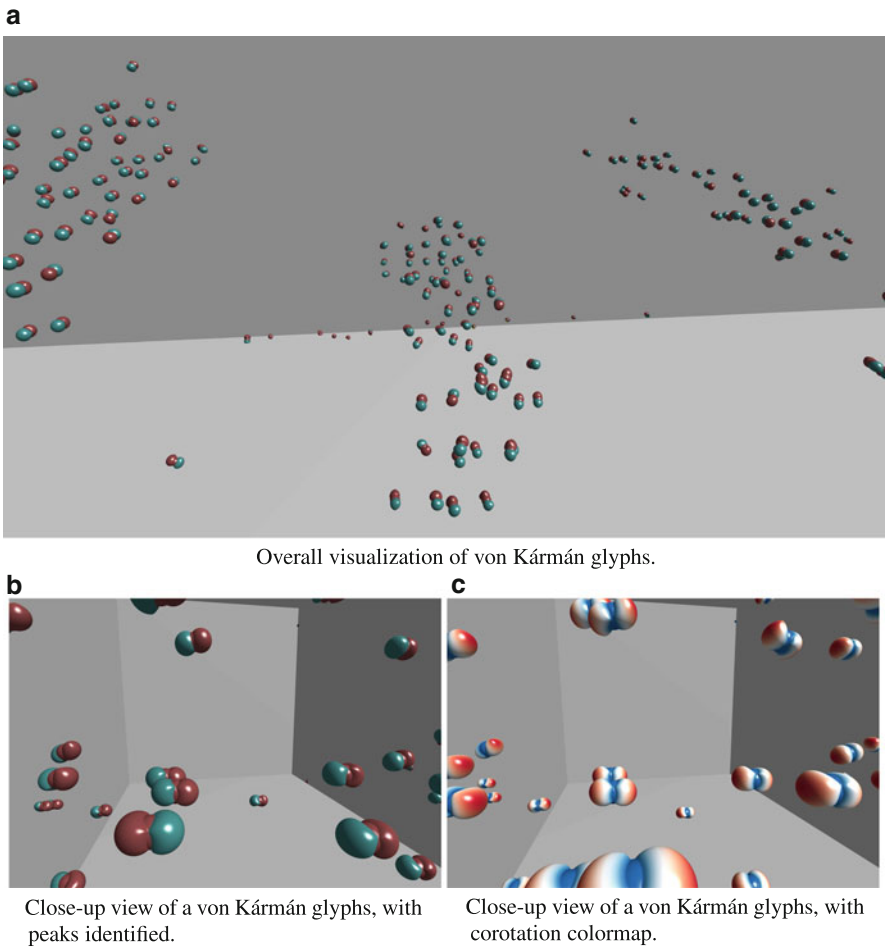

Fig. 6 Visualization of glyphs sampled uniformly in the von Kármán vortex street, as visualized in (**a**). A close-up view of various glyphs is shown in (**b**), (**c**), which show that there exist glyphs that correspond to the canonical "two-peak" examples that mostly point along a uniform direction

6 Conclusions and Future Work

In this work we have introduced glyph-based visualization of corotation-based vortices. We have shown how topological analysis of these glyphs both visually and in an automatic fashion can reveal complex vortex behaviors, such as interactions between rotational components present in a single core. In the future we hope to represent the corotation function using multiple levels of detail in order to sample the function more effectively, and investigate how one can extract glyphs in time-dependent flows as the current method applies to discrete time steps. Furthermore, we hope to visually represent vortex core splits and merges in conjunction with the glyphs to investigate a possible relationship between the two.

Acknowledgements This work was partially supported by the Materials Design Institute, funded by the UC Davis/LANL Research Collaboration (LANL Agreement No. 75782-001-09). It was also supported by the NSF under contracts IIS 0916289 and IIS 1018097, the Office of Advanced Scientific Computing Research, Office of Science, of the US DOE under Contract No. DE-FC02-06ER25780 through the SciDAC programs VACET, and contract DE-FC02-12ER26072, SDAV Institute. We thank Simon Stegmaier for making available his software [16].

References

1. V. Kolář, P. Moses, J. Sistek, Local corotation of line segments and vortex identification, in *Proceedings of the Seventeenth Australasian Fluid Mechanics Conference*, Auckland, ed. by G. Mallinson, J. Cater (2010), pp. 251–254
2. J.C.R. Hunt, A. Wray, P. Moin, Eddies, stream, and convergence zones in turbulent flows. Center for Turbulence Research Report CTR-S88, 1988, pp. 193–208
3. U. Dallmann, Topological structures of three-dimensional vortex flow separation, in *16th American Institute of Aeronautics and Astronautics, Fluid and Plasma Dynamics Conference*, Danvers, 1983
4. H. Vollmers, H. Kreplin, H. Meier, Separation and vortical-type flow around a prolate spheroid-evaluation of relevant parameters, in *Proceedings of the AGARD Symposium on Aerodynamics of Vortical Type Flows in Three Dimensions*, Rotterdam, 1983, pp. 14-1–14-14
5. M. Chong, A. Perry, B. Cantwell, A general classification of three-dimensional flow fields. Phys. Fluids **2**, 765–777 (1990)
6. J. Jeong, F. Hussain, On the identification of a vortex. J. Fluid Mech. **285**, 69–94 (1995)
7. V. Kolář, Vortex identification: new requirements and limitations. Intern. J. Heat Fluid Flow **28**(4), 638–652 (2007)
8. M. Roth, R. Peikert, A higher-order method for finding vortex core lines, in *Proceedings of the Conference on Visualization'98*, Minneapolis (IEEE, 1998), pp. 143–150
9. D. Sujudi, R. Haimes, Identification of swirling flow in 3D vector fields, in *AIAA 12th Computational Fluid Dynamics Conference Paper*, San Diego, 1995, pp. 95–1715.
10. D. Kenwright, R. Haimes, Automatic vortex core detection. IEEE Comput. Graph. Appl. **18**, 70–74 (1998)
11. B. Singer, D. Banks, A predictor-corrector scheme for vortex identification. Technical report, TR-94–11, 1994
12. D. Banks, B. Singer, Vortex tubes in turbulent flows: identification, representation, reconstruction, in *Proceedings of the Conference on Visualization'94*, Washington, DC (IEEE, 1994), pp. 132–139
13. D.C. Banks, B.A. Singer, A predictor-corrector technique for visualizing unsteady flow. IEEE Trans. Vis. Comput. Graph. **1**, 151–163 (1995)
14. J. Sahner, T. Weinkauf, H. Hege, Galilean invariant extraction and iconic representation of vortex core lines, in *IEEE VGTC Symposium on Visualization*, Leeds, 2005, pp. 151–160
15. J. Sahner, T. Weinkauf, N. Teuber, H.C. Hege, Vortex and strain skeletons in eulerian and lagrangian frames. IEEE Trans. Vis. Comput. Graph. **13**(5), 980–990 (2007)
16. S. Stegmaier, U. Rist, T. Ertl, Opening the can of worms: an exploration tool for vortical flows, in *IEEE Visualization Conference*, Minneapolis, 2005, pp. 463–470
17. T. Schafhitzel, D. Weiskopf, T. Ertl, Interactive investigation and visualization of 3D vortex structures, in *Electronic Proceedings of 12th International Symposium on Flow Visualization*, Gottingen, Sept 2006
18. T. Schafhitzel, J. Vollrath, J. Gois, D. Weiskopf, A. Castelo, T. Ertl, Topology-preserving $\lambda 2$-based vortex core line detection for flow visualization, in *Computer Graphics Forum*, vol. 27 (Wiley Online Library, 2008), pp. 1023–1030

19. K. Baysal, T. Schafhitzel, T. Ertl, U. Rist, Extraction and visualization of flow features, in *Imaging Measurement Methods for Flow Analysis*. Volume 106 of Notes on Numerical Fluid Mechanics and Multidisciplinary Design, ed. by W. Nitsche, C. Dobriloff (Springer, Berlin/Heidelberg, 2009), pp. 305–314
20. F.H. Post, B. Vrolijk, H. Hauser, R.S. Laramee, H. Doleisch, The state of the art in flow visualisation: feature extraction and tracking. Comput. Graph. Forum **22**, 775–792 (2003)
21. M. Jiang, R. Machiraju, D. Thompson, Detection and visualization of vortices, in *The Visualization Handbook*, ed. by C.D. Hansen, C.R. Johnson (Elsevier, Amsterdam, 2005), pp. 295–309
22. C. Garth, X. Tricoche, T. Salzbrunn, T. Bobach, G. Scheuermann, Surface techniques for vortex visualization, in *VisSym*, Konstanz, 2004, pp. 155–164
23. M. Jankun-Kelly, M. Jiang, D. Thompson, R. Machiraju, Vortex visualization for practical engineering applications. IEEE Trans. Vis. Comput. Graph. **12**(5), 957–964 (2006)
24. X. Tricoche, C. Garth, G. Kindlmann, E. Deines, G. Scheuermann, M. Ruetten, C. Hansen, Visualization of intricate flow structures for vortex breakdown analysis, in *Proceedings of the Conference on Visualization, VIS'04*, Washington, DC (IEEE, 2004), pp. 187–194
25. C.D. Shaw, D.S. Ebert, J.M. Kukla, A. Zwa, I. Soboroff, D.A. Roberts, Data visualization using automatic perceptually motivated shapes, in *SPIE Conference on Visual Data Exploration and Analysis*, San Jose, 1998, pp. 208–213
26. F.H. Post, F.J. Post, T.V. Walsum, D. Silver, Iconic techniques for feature visualization, in *Proceedings of the 6th Conference on Visualization, VIS'95*, Washington, DC (IEEE, 1995), pp. 288–295
27. A. Wiebel, S. Koch, G. Scheuermann, Glyphs for non-linear vector field singularities, in *Topological Methods in Data Analysis and Visualization II*, ed. by R. Peikert, H. Hauser, H. Carr, R. Fuchs. Mathematics and Visualization (Springer, Berlin/Heidelberg, 2012), pp. 177–190
28. G. Kindlmann, Superquadric tensor glyphs, in *Proceedings of the Sixth Joint Eurographics – IEEE TCVG Conference on Visualization, VISSYM'04*, Aire-la-Ville (Eurographics Association, 2004), pp. 147–154
29. T. Schultz, C.F. Westin, G. Kindlmann, Multi-diffusion-tensor fitting via spherical deconvolution: a unifying framework, in *Proceedings of the 13th International Conference on Medical Image Computing and Computer-Assisted Intervention: Part I, MICCAI'10*, Beijing (Springer, Berlin/Heidelberg, 2010), pp. 674–681
30. T. Schultz, Towards resolving fiber crossings with higher order tensor inpainting, in *New Developments in the Visualization and Processing of Tensor Fields*, ed. by D.H. Laidlaw, A. Vilanova. Mathematics and Visualization (Springer, Berlin/Heidelberg, 2012), pp. 253–265
31. T. Peeters, V. Prckovska, M. van Almsick, A. Vilanova, B. ter Haar Romeny, Fast and sleek glyph rendering for interactive hardi data exploration, in *Visualization Symposium, PacificVis'09*, Beijing (IEEE, Apr 2009), pp. 153–160
32. M. van Almsick, T.H. Peeters, V. Prčkovska, A. Vilanova, B. ter Haar Romeny, GPU-based ray-casting of spherical functions applied to high angular resolution diffusion imaging. IEEE Trans. Visual. Comput. Graph. **17**(5), 612–625 (2011)
33. R. Borgo, J. Kehrer, D.H.S. Chung, E. Maguire, R.S. Laramee, H. Hauser, M. Ward, M. Chen, Glyph-based visualization: foundations, design guidelines, techniques and applications, in *Eurographics State of the Art Reports* (EG STARs, Eurographics Association, May 2013), pp. 39–63. http://diglib.eg.org/EG/DL/conf/EG2013/stars/039-063.pdf
34. T. Schultz, G. Kindlmann, A maximum enhancing higher-order tensor glyph. Comput. Graph. Forum **29**(3), 1143–1152 (2010)
35. S. Beucher, F. Meyer, The morphological approach to segmentation: the watershed transformation (Mathematical morphology in image processing). Opt. Eng. **34**, 433–481 (1993)
36. H. Carr, J. Snoeyink, U. Axen, Computing contour trees in all dimensions. Comput. Geom. Theory Appl. **24**(2), 75–94 (2003)
37. C. Hung, P. Buning, Simulation of blunt-fin-induced shock-wave and turbulent boundary-layer interaction. J. Fluid Mech. **154**(1), 163–185 (1985)